On the Aerodynamics of Paper Airplanes

Conference Paper · June 2009

DOI: 10.2514/6.2009-3958

4 authors, including:

Bing Feng NG
Nanyang Technological University
59 PUBLICATIONS **374** CITATIONS
SEE PROFILE

Yin Yin Pey
Nanyang Technological University
7 PUBLICATIONS **29** CITATIONS
SEE PROFILE

Jorg Schluter
Deakin University
66 PUBLICATIONS **899** CITATIONS
SEE PROFILE

27th AIAA Applied Aerodynamics Conference
22 - 25 June 2009, San Antonio, Texas

AIAA 2009-3958

On the Aerodynamics of Paper Airplanes

Ng Bing Feng, Kng Qiao Mei, Pey Yin Yin [*], and Jörg U. Schlüter[†]

Nanyang Technological University, School of Mechanical and Aerospace Engineering, Singapore

The design of Micro Air Vehicles (MAV) is challenging since the aerodynamic efficiency of airfoils and wings decreases at low Reynolds-numbers. While many MAV approaches investigate biological designs, we present an investigation on the aerodynamics of paper airplanes, which fly in the same Reynolds-number range as MAV, but have the advantage of simplicity. We present flow visualizations and force measurements in a water tunnel on the dart paper airplane design.

Nomenclature

C_D	=	drag coefficient
C_L	=	lift coefficient
L/D	=	lift over drag ratio
L	=	lift force
AR	=	aspect ratio
Λ	=	sweep angle
α	=	angle of attack
l	=	length of the airplane
b	=	wing span
S	=	planform area
ρ	=	density
U_∞	=	airspeed
ν	=	kinematic viscosity
Re	=	Reynolds number (Re= $U_\infty \cdot l / \nu$)

[*] Aerospace Engineers
[†] Assistant Professor

I. Introduction

PAPER AIRPLANES are a source of inspiration for all ages and have been the introduction to aeronautical engineering for many generations. The fascination of these airplanes has led to a wide variety of paper airplane designs that stem from countless hours of experimentation. As such, the designs of the paper airplanes have been optimized by trial-and-error through a large number design cycles. Similar to the biological evolutionary process, the most popular designs have shown to be the most performing and the simplest to manufacture.

The current push to design Micro Air Vehicles (MAV) looks often toward biological designs [1] [2], such as flapping wings or morphing wings to improve the inherently limited aerodynamic performance of airfoils and wings at low Reynolds-numbers [3] [4]. However, biological designs are very difficult to copy as the control mechanisms of e.g. an avian wing are very sophisticated. Since MAV are flying in the same Reynolds-number regime as paper airplanes, and since paper airplanes have gone through a large number of experimental design cycles, we are now investigating the aerodynamic performance of paper airplanes in order to identify aerodynamic effects that can aid in the design of MAV. Due to their simplicity, paper airplane designs would be much easier than biological designs to incorporate in to new MAV designs. In the following chapters, we present flight performance tests, flow visualizations and force measurements of paper airplane models.

II. Choice of Airplane Model

There is a wide selection of paper airplane designs that display a good performance. Here, we would like to look at the dart paper airplane design (Figure 1). We have chosen the dart design for its popularity.

The dart design can be achieved by folding a piece of paper along the centerline of the long side. The corners are then folded outwards thrice. At the wing tips, winglets can be folded up.

Using an A4 sized paper sheet, the airplane has a wingspan of about b=0.16 m and a wing area of about S=0.023 m^2, leading to a rather low aspect ratio of AR=1.1. The weight of the airplane is that of an A4 sized piece of paper and can be approximated as 5 grams. The sweep angle is Λ=67°.

Figure 1: Folding procedure to obtain dart paper airplane.

III. Flight Testing

A. Procedure

Before analyzing the aerodynamics of the paper airplane in water tunnel tests, we performed flight tests in order to determine important flight parameters, such as flight speed and lift-to-drag ratio. As there are variations in how the same design can be folded by two persons in a different manner, and as the flight performance is dependent on the fashion of launch, we have chosen to use a statistical approach. We have folded five different test models and used three different test persons for launch. With these models, we have performed 10 flights of each airplane recording flight time and distance traveled. With that, we have determined the flight speed and the lift-over-drag ratio by the glide ratio.

The lift coefficient is then determined by: $C_L = \frac{L}{\frac{1}{2}\rho U_\infty^2 S}$

with the lift force L=0.005kg × 9.81 m/s^2. The lift-to-drag ratio L/D is determined from the distance traveled over the launch height. The drag coefficient can then be determined from the lift coefficient and the lift to drag ratio.

B. Results from the Flight Test

		Flight Speed	*L/D*	C_L	C_D
Plane 1	Average	4.48	4.92	0.19	0.04
	Standard Dev.	1.8039	0.2124	0.0128	0.0007
Plane 2	Average	4.15	4.88	0.23	0.05
	Standard Dev.	1.3472	1.0211	0.0318	0.0024
Plane 3	Average	5.65	4.94	0.12	0.02
	Standard Dev.	2.1897	0.6815	0.0044	0.0002
Plane 4	Average	4.24	5.44	0.22	0.04
	Standard Dev.	1.7929	1.8383	0.0329	0.0022
Plane 5	Average	6.00	5.09	0.11	0.02
	Standard Dev.	2.7683	1.2442	0.0031	0.0001
Total	**Average**	**4.90**	**5.05**	**0.17**	**0.03**
	Standard Dev.	**1.9804**	**0.9995**	**0.0170**	**0.0011**

Table 1: Performance measurements of five different dart paper airplanes.

As can be seen in Table 1, the flight performances of the airplanes differ in flight speed with a smallest average flight speed of 4.1 m/s for Plane 2 and 6.0 m/s for Plane 5. Figure 2 shows the probability density distribution for of all test flights with some flights recording flight speed of below 3 m/s and some more than 9 m/s. However, the vast majority of flights are recorded between 3 and 6 m/s. The lift-over-drag ratio is relatively constant at an *L/D* of about five. The variation of lift coefficient and drag coefficient is also relatively small.

With the flight data available, we can now continue with flow measurements in a water tunnel.

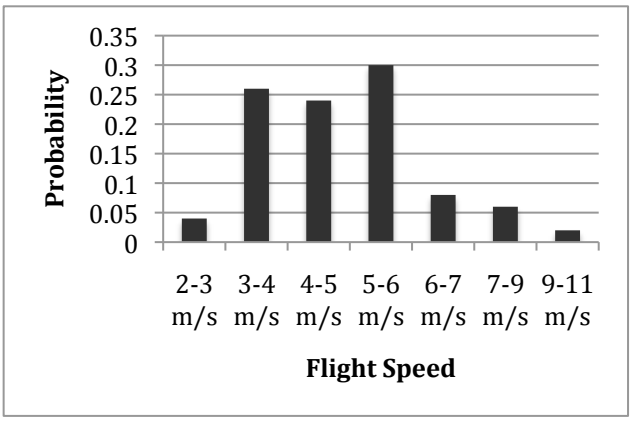

Figure 2: Probability density distribution of the flight speed of all test flights.

IV. Water Tunnel Setup

C. Water Tunnel Facility and Force Balance

We have used a water tunnel for the analysis of the airplane. A water tunnel is an excellent facility to visualize the flow, since the kinematic viscosity is 15 times smaller than that of air. This means, at a constant Reynolds-number and a constant model size, the flow speed of the water is approximately 15 times smaller. Furthermore, the high density of the fluid increases the dynamic pressure, which facilitates the measurement of forces on a model. In our case, the absolute forces measured within the water tunnel are approximately three times larger than in air.

The water tunnel is a model from LongWin with a contraction ratio of 1:6 and a test section size of 0.3 m wide x 0.3 m high x 1.0 m long. The velocity range is from 0-0.65 m/s. The flow uniformity is high, with a maximum velocity change in the core test section of less than 2%.

Forces are measured with a Chroma 3-component force balance measuring lift, drag and moments. The balance was calibrated with static loads before the measurements. The maximum load of the balance is 20 N in lift and drag direction. The accuracy of the load cells is given by the manufacturer as 0.5% of the full load, which translates into a maximum error of 0.1N.

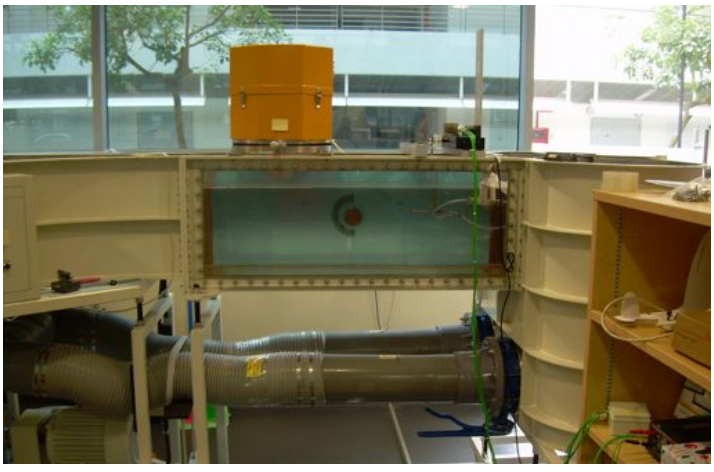

Figure 3: Water tunnel test section with 3-component force balance.

D. Water Tunnel Models

We used two different models for the tests. One full-scale model for flow visualizations and a half-scale model for force measurements. The scaling down of the model was necessary to avoid interference with the walls at high angles of attack. The models are manufactured from folded aluminum of 0.8mm strength. For the full-scale model, in order to maintain Reynolds similarity in the water tunnel, the flow speed needs to be adjusted to 0.3 m/s in water corresponding to a flight speed of about 5 m/s in air. For the half-scale model, a flow speed of 0.6 m/s in water corresponds to real flight conditions. The steel rod holding the model in place contributes to the measured drag. In order to compensate this effect, we have measured the drag of the steel rod itself and deducted the drag force from all measurements. However, the fixture of the model to the rod incurs additional drag that is difficult to account for.

Figure 4: Dart airplane water tunnel models. Left: Force balance model. Right: Flow visualization model.

V. Flow Visualizations

A. Dart paper airplane

We used food dye to visualize the main flow features of the flow around the paper airplane. One of the major flow features of a delta wing is the vortex on the upper side of the wing. Figure 5 shows the flow visualization of that wing vortex at a Reynolds number of Re=55,000. The dye is injected on the edge of the lower side of the wing at a distance of 1/3 of the airplanes length downstream of the tip. The wing vortex is also observable at higher Reynolds numbers, but difficult to visualize and present in still images.

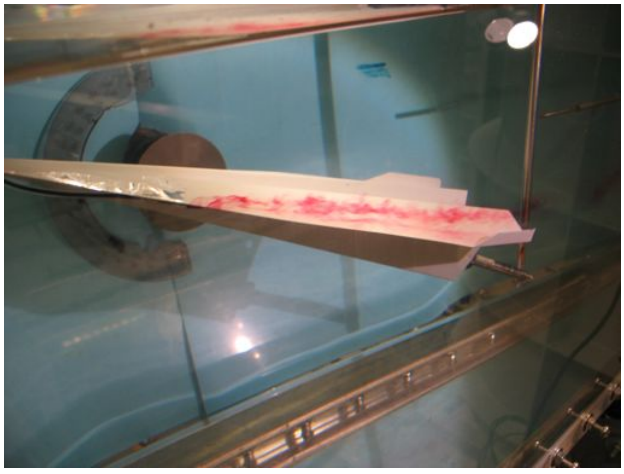

Figure 5: Wing vortex at high angles of attack (Re=55,000).

The main difference of the dart paper airplane and a traditional delta wing is the centerfold. While the centerfold has a number of operational advantages, such as providing a handle for launch and increasing its lateral stability, we would like to assess its influence on the main wing flow. When injecting dye close to the centerfold, we observed that the streamlines have a distinct component toward the center (Figure 6). Since the centerfold opens up toward the tail the massflow rate inside the centerfold increases from its tip toward the tail. As such, it draws mass from the main wing toward the center.

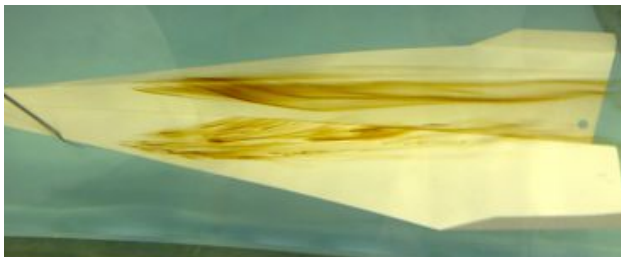

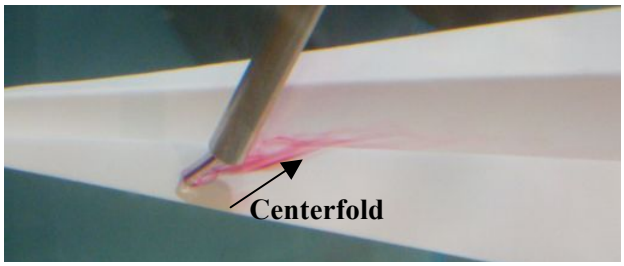

Figure 6: Streamlines close to the centerfold.

In order to assess the influence of the centerfold onto the wing vortex, we have covered the centerfold with clear tape and visualized the flow. Figure 7 juxtaposes the flow visualizations of the model with a covered and open centerfold. It can be observed that the vortex is drawn slightly more toward the center of the airplane by the flow into the centerfold.

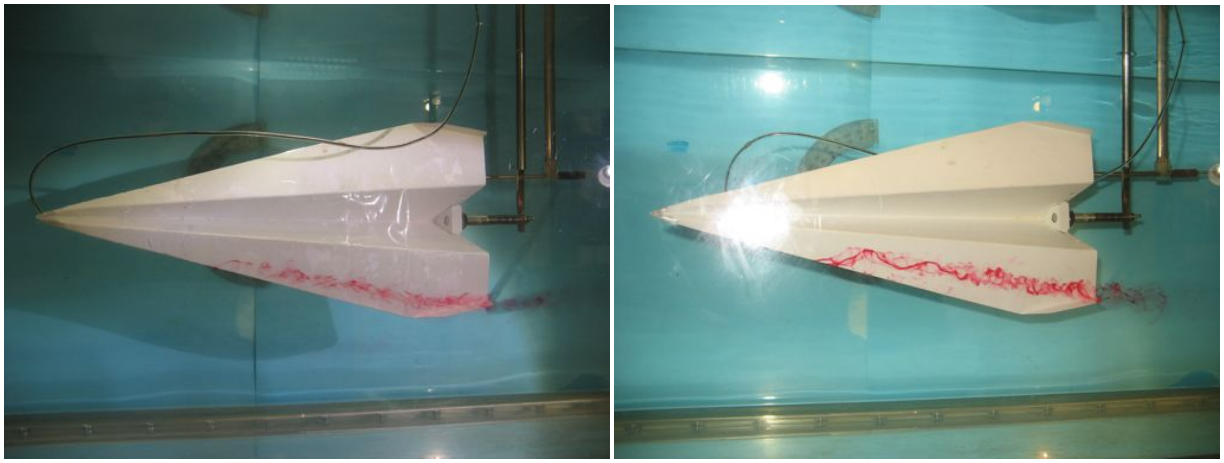

Figure 7: Comparison of wing vortex trajectory (Re=28,000). Left: centerfold covered with clear tape. Right: Original model.

VI. Force Measurements of the Dart Paper Airplane

A. Lift and Drag Curves

In order to quantify the flight performance of the paper airplane, we have measured the lift and drag of the airplane using the scaled model. The Reynolds-number of the flight model based on the length of the

airplane of l=0.297m and the flight speed of U_∞=4.90 m/s is Re=95,000. The scaled down model has a length of l=0.105m. At a flow speed of U_∞=0.6 m/s in water, this amounts to Re=91,000.

Figure 8 shows the lift curve measured for the dart paper airplane. It can be seen that the stall occurs at quite high angles of attack of about α=30°. This is consistent with previous experience with delta wings with high sweep. The wing vortex observed in the flow visualizations energizes the flow on the upper side of the wing and prevents flow separation. For comparison, we have added in Figure 8 the data from Traub *et al.* [5] and Wentz and Kohlman [6].

Traub *et al.* measured the lift curve of a delta wing with a sweep angle of Λ=70° at a Reynolds-number of Re=60,000. Wentz and Kohlman did the same geometry at a higher Reynolds number. As can be seen from the measurements, the influence of the Reynolds-number on sharp edged delta wings is minimal.

In flight tests, we measured an average lift coefficient of C_L=0.17. Figure 8 shows that this corresponds to an average angle of attack of α=5°. The ability of the airplane to create lift at angles of attack much higher than its cruise condition explains the fact that the airplane displays a robust flight behavior, especially to different launch conditions.

Figure 8 also shows the lift-over-drag curve for the airplane. The solid line shows the data from the balance, while the X markers are representing the data from the flight tests. In general, the balance measurements measure a larger drag coefficient than determined in flight tests. This can be associated to the incomplete compensation of the drag due to the fixture of the model in the water tunnel. The uncertainty of the drag measurements is relatively high, as can be seen in the error bars. Since the drag force is a relatively small quantity the load cell of the balance has difficulties resolving the small measured forces

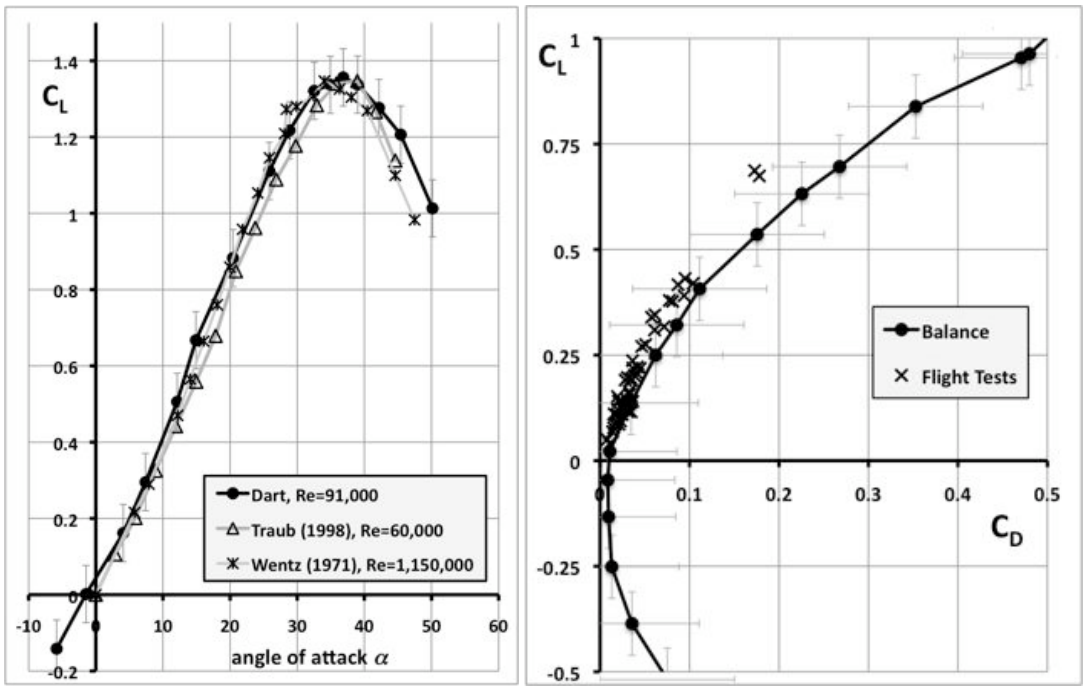

Figure 8: Lift curve of the dart paper airplane in the water tunnel (left hand side) and lift-over-drag plot of the water tunnel model and the flight tests.

B. Influence of Centerfold

Since the flow visualizations showed that the centerfold influences the flow field on the surface of the wings, we tested whether this has an influence on the lift characteristics of the airplane. Again, we have covered the centerfold of the airplane with tape and repeated the lift measurements. Since the covering of the centerfold creates a large bluff body at the trailing edge, the drag increases significantly, and hence the comparison of drag coefficients would not be fair. We will concentrate here on the lift measurements.

Figure 9 shows the lift curves for the uncovered and covered airplane. The airplane with the centerfold shows slightly higher lift coefficients. The displacement of the wing vortex seems to provide a small advantage. However, considering the margin of error of our measurements as displayed in the error bars, the advantage may not be fully conclusive from our measurements alone.

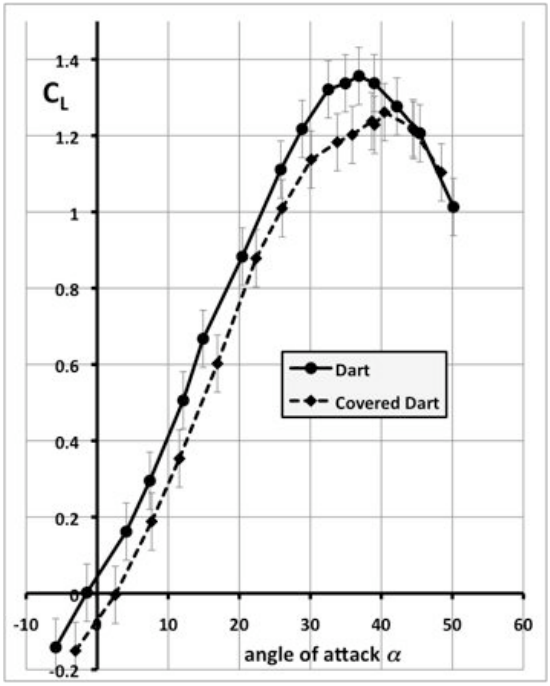

Figure 9: Influence of the centerfold. Diamonds: Original model; Squares: Model with covered centerfold.

VII. Computational Analysis

Since the level of uncertainty of our measurements is relatively high, we initiated a series of computations to solidify our hypothesis. The model that we used is that of a trapezoidal paper airplane, since the pointed tip can cause difficulties in meshing as well as the computation itself. We use three different models:

Model A: The control case is that of a trapezoidal plate (Figure 10).

Model B: The second model possesses a centerfold, but the centre fold and the crease are parallel in the streamwise direction, which means that at zero angle of attack, the entire sheet is aligned with the flow (Figure 11).

Model C: The last model has a larger centerfold, inclining portions of the sheet towards the flow. Hence, at zero angle of attack, this configuration will produce lift, since portions of the centerfold have a positive angle of attack (Figure 12).

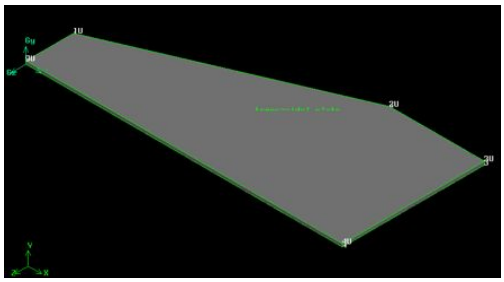

Figure 10: Semi-Model A (control case). The geometry is symmetric in the centerline.

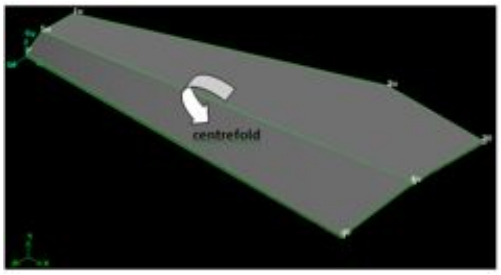

Figure 11: Model B (with centerfold)

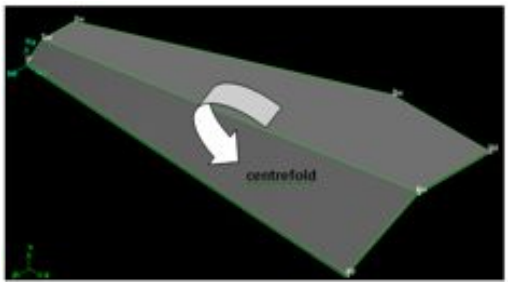

Figure 12: Model C (with steeper centerfold)

The mesh is a structured mesh with 0.95 million mesh points generated with the commercial mesh generator GAMBIT Figure 13. We have established mesh independence by a mesh refinement study.

The solver that we use is the commercial solver Fluent. The solver uses a second order upwind scheme and the Spallart-Allmaras turbulence model. The solution is usually converged to 10^{-5}.

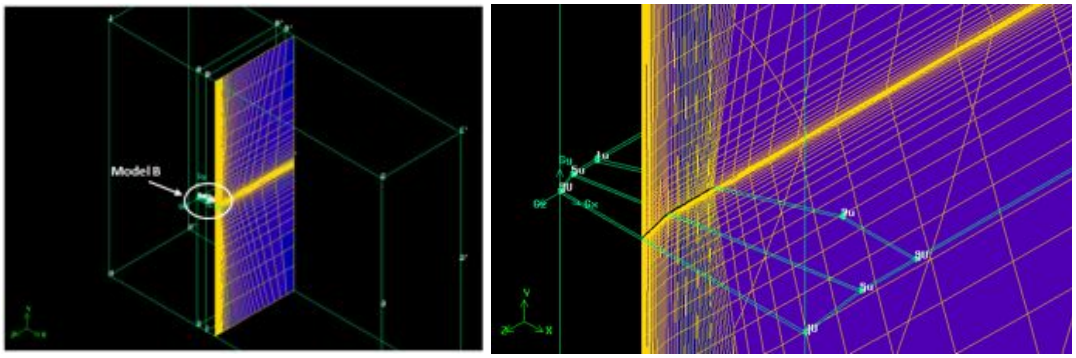

Figure 13: Fine mesh of Model B

The results of the simulations can be seen in Figure 14. Simulations show that there is a small, but persistent advantage of the centerfold model B over the reference case model A. The $C_{L,max}$ increases by about 5%. Model C creates essentially a left-shift, since portions of the model are at a higher angle of attack than the main wing.

The lift-over-drag (Figure 15) shows no significant difference between the models, except for very high lift. Here, the centerfold models have a slightly better lift-to-drag ratio.

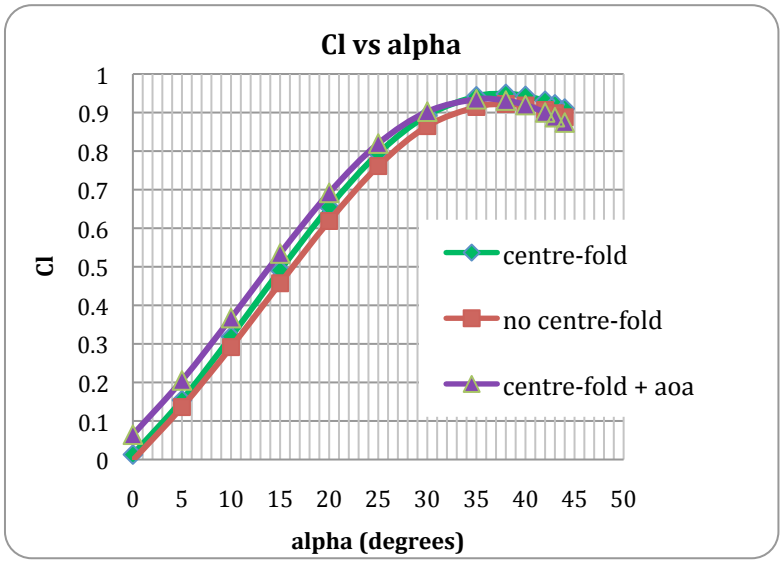

Figure 14: Plot of CL versus alpha – Models A, B and C

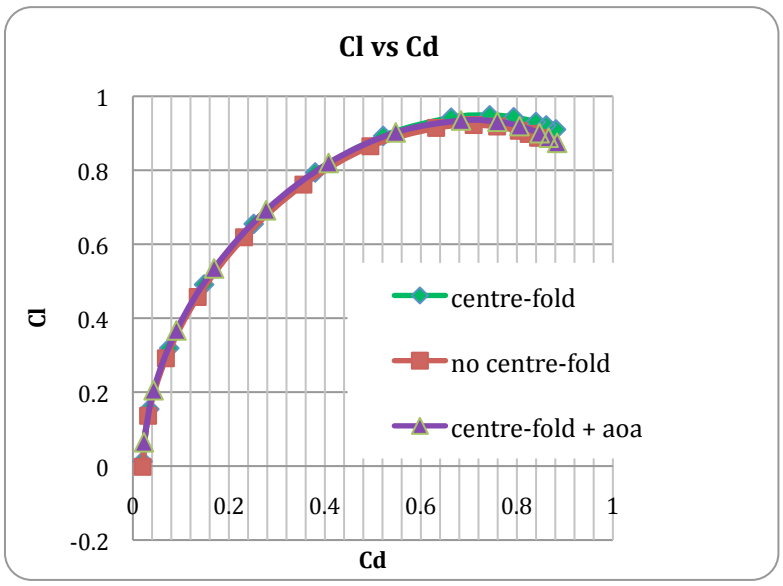

Figure 15: Plot of CL versus CD – Models A, B and C

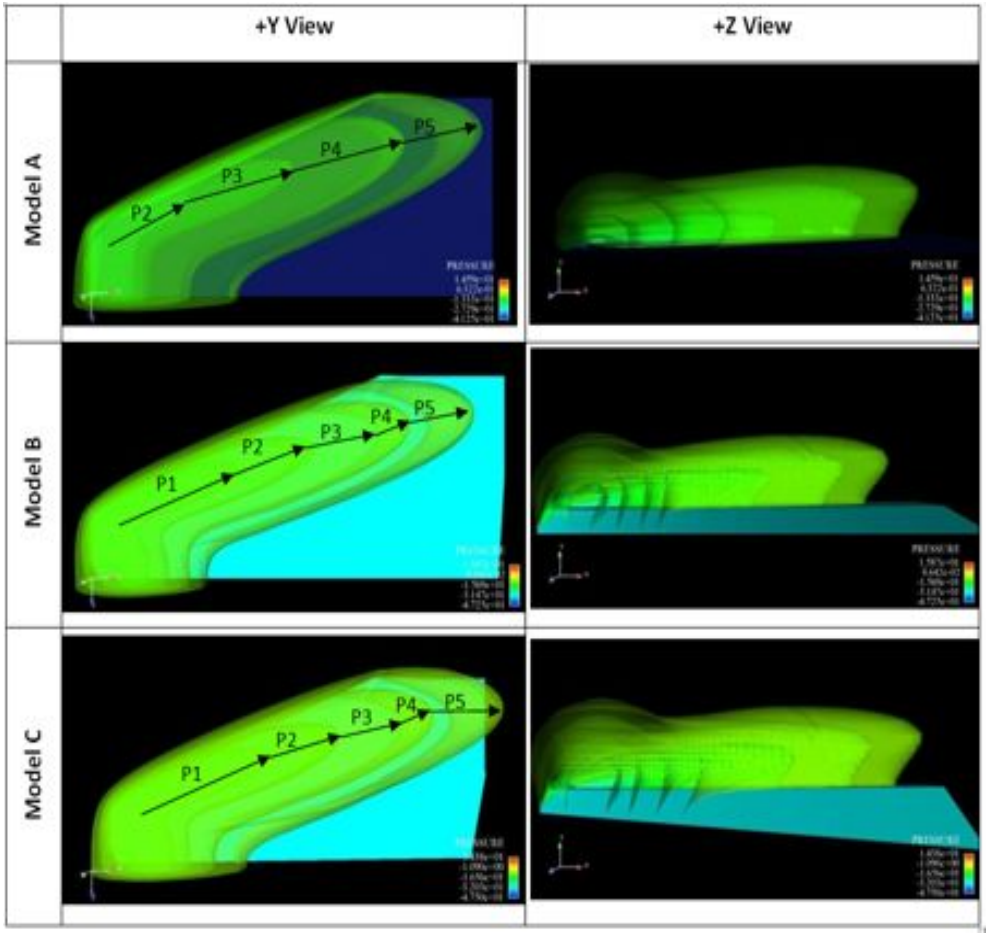

Figure 16: Iso-pressure surfaces of the three models at α=25º

Figure 16 shows the pressure distribution on the wing at high angles of attack. The levels of the pressure isosurfaces are identical for all three pictures. It can be seen that model B and C have more intense vortex with a trajectory slightly bound more inwards that the reference case.

VIII. Conclusions

We have investigated the lift and drag characteristics of a paper airplane in order to determine design recommendations for MAV. We have shown that the dart paper airplane is able to display high lift coefficients over a large range of angle of attacks. We have identified that the centerfold of the paper airplane alters the flow on the upper side of the wing. We have observed that the wing vortex on the upper side of the delta wing is slightly bent toward the centre. We postulated that this extends the low-pressure region on the upper side of the wing. Our water tunnel lift measurements and our computations validate this assumption.

We have shown that the delta wing configuration of a typical paper airplane provides a possible layout for a MAV and provides advantages in terms of high lift capabilities and robust handling qualities. We have also shown that the centerfold, apart from its use as a structural reinforcement and stability in the yaw axis, provides aerodynamic advantages in terms of wing vortex management.

Acknowledgments

We thank the support of the Defence Science Organization Singapore and the NTU Office of Research through the DSO-URECA programme.

References

1. Mueller, T.J.a.D., J. D., *An Overview of Micro Air Vehicle Aerodynamics*, in *Fixed and Flapping Wing Aerodynamics for Micro Air Vehicle Applications*. 2001, AIAA, Progress in Astronautics and Aeronautics. p. 1-10.
2. Jones, K., Duggan, S. J., and Plazer. M. F. , *Flapping Wing Propulsion for a Micro Air Vehicle*, in *39th Aerospace Sciences Meeting and Exhibit*. 2001: Reno, NV.
3. Mueller, T., Kellogg, J. , Ifju, P., Shkarayev, S., *Introduction to the Design of Fixed Wing Micro Air Vehicles.* AIAA Education Series, 2006.
4. Platzer, M., and Jones K., *Flapping Wing Aerodynamics – Progress and Challenges*, in *44th Aerospace Sciences Meeting and Exhibit*. 2006: Reno, NV.
5. Traub , L.W., ; Moeller, Brian ; Rediniotis, Othon, *Low-Reynolds-Number Effects on Delta-Wing Aerodynamics.* Journal of Aircraft, 1998. **35**(4): p. 653-656.

6. Wentz, W.H.K., D. L., *Vortex breakdown on slender sharp-edged wings* Journal of Aircraft, 1971. **8**(3): p. 156-161.